Charge density influence on cold fusion barriers

R. A. Gherghescu, D. N. Poenaru[1,2,*] and W. Greiner[1,2]

[1]*Horia Hulubei National Institute for Physics and Nuclear Engineering, Bucharest-Magurele, P.O.Box MG-6, Romania*

[2]*Institut für Theoretische Physik der J. W. Goethe Universität, Frankfurt am Main, D-60054, Germany*

(Dated: October 17, 2008)

Abstract

Cold fusion barriers are studied with respect to the change of the charge density within the overlapping region. Charge evolution from separated target and projectile up to the compound nucleus is taken into account by meaning of a deduced transition formula which depends on geometric parameter variation defining the shape. Macroscopic, shell correction and total deformation energy for fusion like configurations are calculated for different charge density paths. Minimization along this coordinate produces variations of about 4 MeV for light nuclei and up to 8 MeV for superheavy synthesis, for the deformation energy in the last part of the process.

PACS numbers:

*Horia Hulubei - National Institute for Nuclear Physics and Engineering, P.O.Box MG-6, RO-76900, Bucharest, Romania, E-mail:rgherg@ifin.nipne.ro

I. CHARGE DENSITY VARIATION

The usual procedure to deal with different orientations of the target nucleus is to average the fusion cross section over the all possible angles [1]. However, it is stressed for ex. in [2], that the barrier height for subbarrier fusion reactions increases with the collision angle for prolate deformed nuclei. Here, the value of the angle between the symmetry axis (axes) and collision axis θ=0 ° corresponds to tip to tip collision and produces the lowest Coulomb barrier height (the studied reaction was ^{76}Ge+^{150}Nd). The effective potential is also shown to increase for a change in angular orientation of the ellipsoidally deformed target, when the collision angle increase from 0 ° to 90 ° in ^{238}U+16O reaction [3]. It is also emphasized that, as far as geometrical effects are concerned, when the deformed nucleus symmetry axis is rotated as to be perpendicular to the collision axis, the Coulomb barrier height increases [4]. These considerations lead us to consider only the tip to tip configuration as being energetically the most favourized one. Any deviation ($\theta > 0$ °) produces an increase in the potential barrier. One has to mention however that this is true only for prolate type shapes. For β <0 ° deformations (oblate shapes), the barrier becomes higher when the symmetry axis coincides with the collision one [5]. Therefore a typical nuclear configuration for fusion phenomena is described by two intersected ellipsoids with (a_1, b_1) and (a_2, b_2) semiaxes, separated by a plane $z = z_s$. The two volumes are defined by the shape parameters. We will refer furtheron only to the left side of the shape corresponding to the heavy fragment (A_1, Z_1), the demonstration for the light fragment being similar. Variation of Z_{1x}/A_{1x} must also comply to:

$$(\frac{Z_{1x}}{A_{1x}})_f = \frac{Z_0}{A_0} \tag{1}$$

where Z_0 and A_0 are the final values corresponding to the compound nucleus and:

$$(\frac{Z_{1x}}{A_{1x}})_i = \frac{Z_1}{A_1} \tag{2}$$

where Z_1 and A_1 are the initial values of the target nucleus. A variation law fulfilling these conditions is:

$$\frac{Z_{1x}}{A_{1x}} = \frac{1}{A_0 - A_1}\left[(A_{1x} - A_1)\frac{Z_0}{A_0} + (A_0 - A_{1x})\frac{Z_1}{A_1}\right] \tag{3}$$

The corresponding proton densities are:

$$\rho_{p1} = \frac{Z_{1x}}{V_{1x}} = \frac{Z_{1x}}{\frac{4\pi}{3}a_1 b_1^2}$$
$$\rho_{p2} = \frac{Z_{2x}}{V_{2x}} = \frac{Z_{2x}}{\frac{4\pi}{3}a_2 b_2^2} \tag{4}$$

where $V_{1x} = (4\pi/3)a_1 b_1^2$ and $V_{2x} = (4\pi/3)a_2 b_2^2$ are the volumes of the ellipsoids corresponding to separate nuclei (A_{1x}, Z_{1x}) and (A_{2x}, Z_{2x}).

For the same fusion reaction, an ellipsoidal projectile can change its shape parameters (a_2, b_2) in different ways along the overlapping region: it can preserve its initial b_{20} semiaxis or b_2 can become larger up to the limit where $b_2 = b_0$, the semiaxis of the compound nucleus. Between these two limits, b_2 can take any values, provided that the volume V_2 does not become larger then its initial value. Consequently, the corresponding intermediary atomic number which is proportional to the charge density, Z_{2i} changes according to the above considerations.

II. SINGLE-PARTICLE ENERGY LEVELS

The microscopic potential which follows the equipotentiality on the nuclear surface is generated by the ellipsoidally deformed two center oscillators:

$$V^{(r)}(\rho, z) = \begin{cases} V_1(\rho, z) = \frac{1}{2}m_0\omega_{\rho_1}^2\rho^2 + \frac{1}{2}m_0\omega_{z_1}^2(z+z_1)^2 \ , v_1 \\ V_2(\rho, z) = \frac{1}{2}m_0\omega_{\rho_2}^2\rho^2 + \frac{1}{2}m_0\omega_{z_2}^2(z-z_2)^2 \ , v_2 \end{cases} \tag{5}$$

where v_1 and v_2 are the space regions where the two potentials are acting.

Besides the overlapped deformed oscillator energies, charge density acts on the angular momentum dependent interactions. In order to assure hermicity of the matrices (due to the fact that strength parameters have specific values varying with the mass number), the anticommutator is used to obtain the spin-orbit and the $\mathbf{l^2}$ term :

$$V_{so} = \begin{cases} -\left\{\frac{\hbar}{m_0\omega_{01}}\kappa_1(\rho, z), (\nabla V^{(r)} \times \mathbf{p})\mathbf{s}\right\} \ , v_1 - region \\ -\left\{\frac{\hbar}{m_0\omega_{02}}\kappa_2(\rho, z), (\nabla V^{(r)} \times \mathbf{p})\mathbf{s}\right\} \ , v_2 - region \end{cases} \tag{6}$$

and similarly for the $V_{\mathbf{l^2}}$ term. It is important to observe that with the above form, the spin-orbit potential becomes shape dependent through the $\nabla V^{(r)}$ term.

The spin-orbit operator is calculated as usual using creation and anihilation components:

$$\mathbf{\Omega s} = \frac{1}{2}(\mathbf{\Omega}^{+}\mathbf{s}^{-} + \mathbf{\Omega}^{-}\mathbf{s}^{+}) + \mathbf{\Omega}_{z}\mathbf{s}_{z} \tag{7}$$

Strength parameters $\kappa_i(\rho, z)$ depend on the mass region and each of these regions corresponds to v_1 and v_2 space domains. For the same region v_i we have a different κ_i for protons and neutrons. As v_1, v_2 are determined by $V_1(\rho, z) = V_2(\rho, z)$, when frequencies (i.e. ellipsoid semiaxies) vary, so do the matrix elements of $\mathbf{\Omega s}$, in direct correspondence with charge density variation. The result is characterized by different proton and neutron level schemes for various charge density paths. Detailed matrix elements and level scheme calculation are described in [6]. The independent quantities during the overlapping process are χ_1, χ_2 and b_1 and b_2.

The level scheme sequence of the overlapping configurations through the fusion path is used as input for the calculation of the shell correction energy E_{shell}. Strutinsky method [7] is used separately for protons and neutrons, as corresponding to different nucleon numbers and different spin-orbit strenght parameters κ. Mass number dependent κ_p and κ_n for protons and neutrons respectively acts on Z_{2i} and N_{2i}. As a result, E_{shell} is calculated as charge density dependent.

III. MACROSCOPIC ENERGY

The macroscopic energy E_{macro} is computed as the sum of the Coulomb E_C and and the nuclear Yukawa-plus-expoenential term E_Y .

For our two intersected nuclei system shape, the Coulomb energy can be written as [8]:

$$E_C = \frac{2\pi}{3}(\rho_{e1}^2 F_{C1} + \rho_{e2}^2 F_{C2} + 2\rho_{e1}\rho_{e2}F_{C12}) \tag{8}$$

where:

$$F_{C1} \; = \int_{-a_1}^{z_s} dz \int_{-a_1}^{z_s} dz\prime F_1(z, z\prime) \tag{9}$$

The Yukawa-plus-exponential energy E_Y is:

$$E_Y = \frac{1}{4\pi r_0^2}[c_{s1}F_{EY1} + c_{s2}F_{EY2} + 2(c_{s1}c_{s2})^{1/2}F_{EY12}] \tag{10}$$

where:

$$F_{EY1} = \int_0^{2\pi} \int_{-a_1}^{z_s} \int_{-a_1}^{z_s} F_{Y1}^{(1)} F_{Y2}^{(1)} Q^{(1)} d\phi dz dz\prime \tag{11}$$

The total macroscopic deformation energy is:

$$E_{macro} = (E_C - E_C^{(0)}) + (E_Y - E_Y^{(0)}) \tag{12}$$

IV. RESULTS AND DISCUSSION

A superheavy synthesis reaction is analyzed, ^{54}Cr+^{238}U$\rightarrow^{292}$116. Both target and projectile are deformed with $\beta_2^{(^{54}Cr)}$=0.180 and $\beta_2^{(^{238}U)}$=0.215. The superheavy ^{292}116 is considered spherical, with radius $R_0(^{292}116)$=6.63 fm. This is due to the fact that lower E_C corresponds to higher E_Y for the same b_2 law of variation, like it is easy visible for $b_2 = R_0(^{292}116)$ curve. The lowest values for E_{macro} are obtained for $b_2 = R_0(^{292}116)$ curve at the end of fusion. Shell effects do not change the order. The $b_2 = R_0(^{292}116)$ curve for E_{shell} (Fig. 1, upper plot) has not always the lowest values: at the beginning of the overlapping region it is the $b_2 = b_{20}(^{54}\mathrm{Cr})$ path which produce lower shell corrections. Then all four variation curves mix. At the end, again $b_2 = R_0(^{292}116)$ is favourized. This trend is transmitted to the total deformation energy E_b (Fig. 1, lower plot). Close to the tangent point the $b_2 = b_{20}(^{54}\mathrm{Cr})$ curve displays lower E_b values. It is the situation where ^{54}Cr keeps its semiaxis ratio *and* b_2 at its initial values. This part corresponds to the highest charge density, the initial charge density value of the projectile. Around $(R-R_f)/(R_t-R_f)$=0.4 the small semiaxis tends to increase toward $R_0(^{292}116)$. This volume enhancement induces the charge density decrease down to the synthesized superheavy ρ_e - value. Differences between curves reach 8 MeV, a rather large value for the cold fusion total deformation energy variation.

All the above results demonstrate the necessity of taking into account the charge density as a free parameter. Its influence is directly related to geometrical characteristics of the fusion-like shape, as the semiaxis ratio χ and the small semiaxis b_2 quantities. Minimization against these two parameters produce a significant decrease in barrier height.

The deformation energy takes low enough values to counteract the increase of the R_3R_3-term. Consequently, the neck with a large radius is not favourable for the mass tensor neck–

dependent components to lower the action integral, but the deformation energy decreases more drastically so as to determine the final fission path.

The final path for another reaction obtained by multidimensional minimization is plotted on the corresponding contour map in fig. 2. It starts with low R_3 values close to parent configuration, goes through larger neck radii and reaches the scission point ($R - R_i \approx 13$ fm) at $R_3 \approx 6.5$ fm. This result agrees with the neck rupture hypothesis where the neck brakes suddenly at a non–zero value. The valley around a pair (A_H, A_L) of (144, 92) has been obtained and is very close to the result reported. Other pairs like (142, 94) and (140, 96) are also belonging to this fission valley. Their probability of occurence is at least partially due to the shell correction minima generated by the introduction of a smooth microscopic neck potential between fragments.

V. CONCLUSION

Charge density influence on cold fusion barriers manifests itself through geometrical parameters characterizing the target and projectile nuclei within the overlapping region. Changes of semiaxis ratios and magnitude triggers a modification in proton density over the non-overlapped volume of the projectile. As a free coordinate, charge density can lower the cold fusion deformation energy, as a result of minimization against b_2 and χ_2. This kind of influence is especially active in the last part of the fusion process, when the projectile is already half embedded in the target (R_n <0.5) up to total synthesis. Energy differences in the cold fusion channel barrier of $^{292}116$ reach about 8 MeV in the last part of the overlapping process as a result of energy minimization.

Acknowledgements

This work was supported by Ministry of Education and Research, IDEI Program, Project 160, Bucharest.

---

[1] C. Y. Wong, Phys. Rev. Lett. **31**, 766 (1973).

[2] K. Nishio, H. Ikezoe, S. Mitsuoka and J. Lu, Phys. Rev. **C62**: 014602 (2000).

[3] L. C. Vaz and J. M. Alexander, Phys. Rev. **C10**, 464 (1974).

[4] A. S. Jensen and C. Y. Wong, Phys. Rev. **C1**, 1321 (1970).

[5] W. Scobel, A. Mignerey, M. Blann and H. H. Gutbrod, Phys. Rev. **C11**, 1701 (1975).

[6] R. A. Gherghescu, Phys. Rev. **C67**: 014309 (2003).

[7] V. Strutinsky, Nucl. Phys. **A95**, 420 (1967).

[8] D. N. Poenaru, M. Ivascu and D. Mazilu, Comp. Phys. Comm. **19**, 205 (1980).

FIGURE captions

Figure 1 Shell correction E_{shell} (upper plot) and fusion barrier E_b for the four paths in the synthesis of $^{292}116$.

Figure 2 Dynamical path for the ^{92}Se+^{144}Nd reaction in the R, R_3 space of deformation.

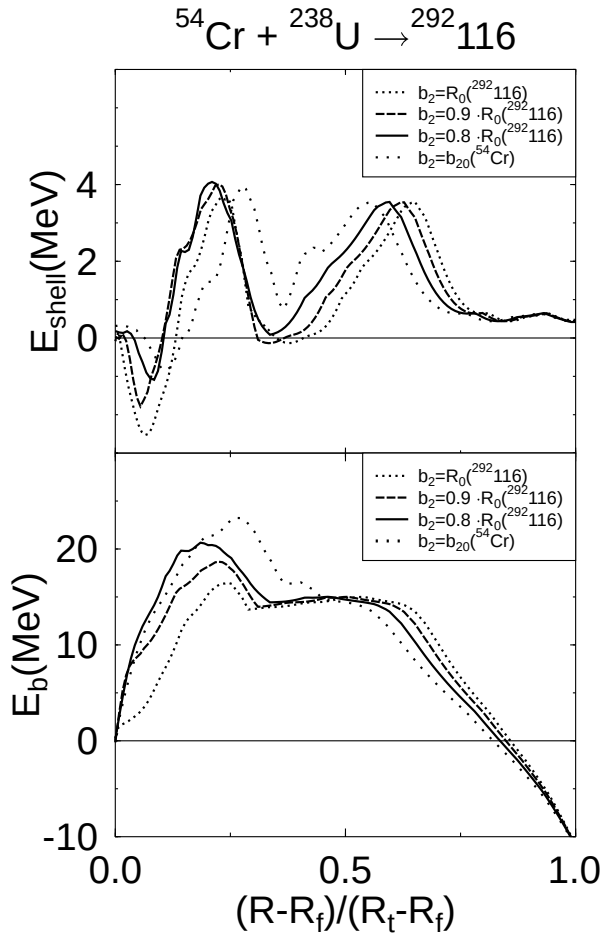
$^{54}Cr + {}^{238}U \rightarrow {}^{292}116$
$b_2=R_0(^{292}116)$
$b_2=0.9\cdot R_0(^{292}116)$
$b_2=0.8\cdot R_0(^{292}116)$
$b_2=b_{20}(^{54}Cr)$
E_{shell}(MeV)
4
2
0
E_b(MeV)
20
10
0
-10
0.0
0.5
1.0
$(R-R_f)/(R_t-R_f)$

Figure 1

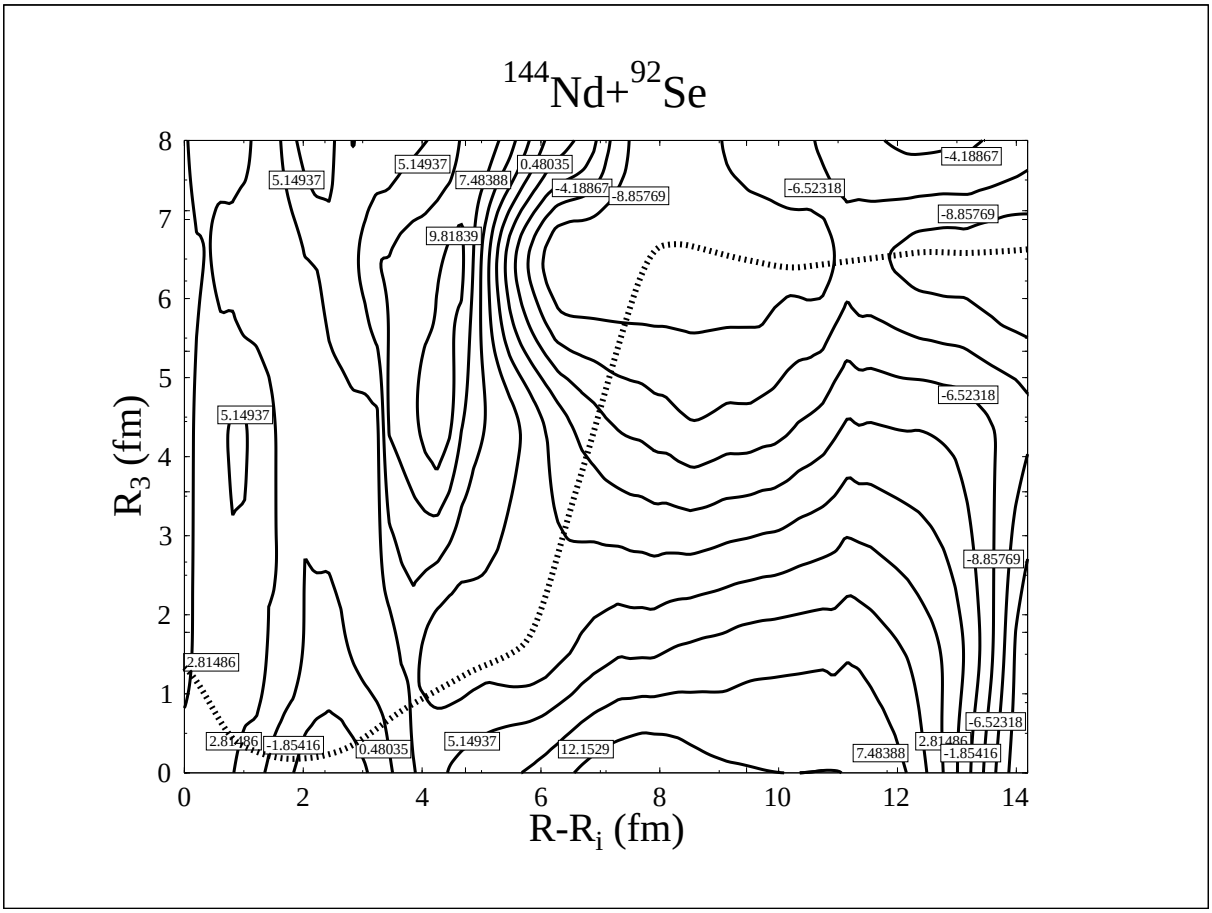
^{144}Nd+^{92}Se
R$_3$ (fm)
R-R$_i$ (fm)
0
1
2
3
4
5
6
7
8
0
2
4
6
8
10
12
14
5.14937
5.14937
7.48388
0.48035
-4.18867
-8.85769
-6.52318
-4.18867
-8.85769
9.81839
5.14937
-6.52318
-8.85769
2.81486
-6.52318
2.81486
-1.85416
0.48035
5.14937
12.1529
7.48388
2.81486
-1.85416

Figure 2

Published articles in stage 2 of the Project 160 - IDEI:

1. R. A. Gherghescu, D. N. Poenaru and W. Greiner
Physical Review C78, 024604 (2008).

2. R. A. Gherghescu, D. N. Poenaru and N. Carjan
Physical Review C77, 044607 (2008).

3. R. A. Gherghescu, D. N. Poenaru and W. Greiner
Invite lecture, International Conference SOTANCP08, Strasbourg, France, June 2008.